AIAA JOURNAL
Vol. 44, No. 2, February 2006

Application of a Nonlinear Computational Aeroacoustics Code to the Gust-Airfoil Problem

R. Hixon*
University of Toledo, Toledo, Ohio 43606
V. Golubev† and R. R. Mankbadi‡
Embry-Riddle Aeronautical University, Daytona Beach, Florida 32114
J. R. Scott§
NASA John H. Glenn Research Center at Lewis Field, Cleveland, Ohio 44135
S. Sawyer¶
University of Akron, Akron, Ohio 44325
and
M. Nallasamy**
QSS Group, Inc., Cleveland, Ohio 44135

A time-domain solution of the gust-airfoil problem is obtained using a high-accuracy computational aeroacoustics code to solve the nonlinear Euler equations. For computational efficiency, the equations are cast in chain-rule curvilinear form, and a structured multiblock solver is used on a distributed-memory parallel computer cluster. To fully investigate the performance of this solver, a test matrix of benchmark problems is computed (two airfoil geometries and four gust-reduced frequencies). These results are compared to benchmark solutions both on the airfoil surface and in the flow domain.

I. Introduction

COMPUTATIONAL aeroacoustics (CAA) is concerned with the time-accurate solution of flow and acoustic phenomena over long periods of time. In the problems of interest, the flow has a range of length and timescales, and bodies with complex geometry are in the computational domain. To accurately compute such complex unsteady problems, high-order finite difference schemes and optimized schemes have been developed, as well as high-accuracy boundary conditions. For an overview of the CAA field, the reader is referred to two excellent review papers[1,2] and a recent special issue of a journal devoted to recent progress in the CAA field.[3]

One practical problem of interest is the unsteady aerodynamics and noise generation that occurs when a periodic vortical gust convecting from upstream impinges on an airfoil. Unsteady flows of this type occur in many practical applications such as fans, wind turbines, helicopter rotors, and turbomachinery. The original analysis techniques for such flows were developed by modeling the airfoil as an infinitely thin flat plate and linearizing the governing equations about a uniform mean flow.[4,5] This analysis neglects the effects of the distortion of the vortical gust caused by the mean flow about an airfoil with thickness, camber, or angle of attack, which proved to have a significant effect on the unsteady lift and noise radiation.[6,7] For an overview of the analysis methods used for this problem, the reader is referred to the review paper by Atassi.[8]

In the past, the gust-airfoil interaction problem has been solved numerically by finite difference linearized Euler solvers in the frequency-domain by Scott and Atassi.[9,10] In the time domain, it has been solved for flat plates using linearized potential equations by Hariharan et al.[11] and using full nonlinear Euler equations by Lockard and Morris.[12] Lockard and Morris have also extended their nonlinear Euler work to NACA 0006 and 0012 airfoil geometries, both lifting and nonlifting[13]; however, they could only compare the results to the solutions obtained with those from flat-plate analysis.

In recent years, Scott has provided benchmark solutions for the problem of a linear vortical gust impinging on a Joukowski airfoil using the GUST3D code.[14,15] These solutions give the steady and unsteady pressure distributions on the airfoil surface as well as the radiated noise directivity in the near field. As a result, these solutions have been used as the basis for validating the new generation of computational aeroacoustics codes, providing a realistic test of the accuracy of these codes on nonuniform flows about complex geometries. Because GUST3D is a linearized Euler equation solver, the mean flow must be specified by the user. In the benchmark solutions, FLO36[16] is used to obtain the mean flows about the airfoils.

The present work documents the results obtained by the NASA BASS computational aeroacoustics code on this set of benchmark problems. BASS is a time-domain nonlinear flow solver, using a block-structured approach to solve the Euler or Navier–Stokes equations in generalized curvilinear coordinates. BASS has been validated for its intended use on turbomachinery problems (e.g., Refs. 17–19), but is designed to be a fully general high-accuracy unsteady flow solver. The goal of this work is to investigate the current applicability of such high-accuracy nonlinear time-domain solvers for realistic external flow calculations.

II. Mathematical and Numerical Formulation

In this work, the two-dimensional nonlinear Euler equations are solved. In Cartesian coordinates these equations are written as

$$\frac{\partial \boldsymbol{Q}}{\partial t} + \frac{\partial E}{\partial x} + \frac{\partial F}{\partial y} = 0 \tag{1}$$

Presented as Paper 2001-1103 at the AIAA 39th Aerospace Sciences Meeting, Reno, NV, 8–11 January 2001; received 30 June 2003; revision received 26 September 2005; accepted for publication 26 September 2005.

*Assistant Professor, Mechanical, Industrial, and Manufacturing Engineering Department. Member AIAA.
†Associate Professor, Aerospace Engineering Department. Senior Member AIAA.
‡Dean, College of Engineering. Associate Fellow AIAA.
§Senior Research Scientist, Acoustics Branch. Senior Member AIAA.
¶Associate Professor, Mechanical Engineering Department. Member AIAA.
**Senior Research Engineer. Senior Member AIAA.

where $\boldsymbol{Q}$ is the vector of conserved properties and E and F are the inviscid flux terms:

$$\boldsymbol{Q} = \begin{Bmatrix} \rho \\ \rho u \\ \rho v \\ E_{\text{tot}} \end{Bmatrix}, \quad E = \begin{Bmatrix} \rho u \\ \rho u^2 + p \\ \rho uv \\ u(E_{\text{tot}} + p) \end{Bmatrix}, \quad F = \begin{Bmatrix} \rho v \\ \rho uv \\ \rho v^2 + p \\ v(E_{\text{tot}} + p) \end{Bmatrix} \tag{2}$$

where

$$E_{\text{tot}} = p/(\gamma - 1) + \rho(u^2 + v^2), \qquad \gamma = 1.4 \tag{3}$$

To apply BASS to realistic complex-geometry flow problems, the equations were recast in generalized curvilinear coordinates:

$$\xi = \xi(x, y), \qquad \eta = \eta(x, y) \tag{4}$$

From previous numerical tests,[20] the chain-rule formulation was chosen as the most accurate form of the equations in three dimensions. The chain-rule curvilinear Euler equations are written as

$$\frac{\partial \boldsymbol{Q}}{\partial t} + \frac{\partial \xi}{\partial x}\left(\frac{\partial E}{\partial \xi}\right) + \frac{\partial \xi}{\partial y}\left(\frac{\partial F}{\partial \xi}\right) + \frac{\partial \eta}{\partial x}\left(\frac{\partial E}{\partial \eta}\right) + \frac{\partial \eta}{\partial y}\left(\frac{\partial F}{\partial \eta}\right) = 0 \tag{5}$$

The time-stepping method used was the low storage fourth-order nonlinear extension of Hu's 5-6 low dispersion and dissipation Runge–Kutta scheme[21] by Stanescu and Habashi.[22]

The spatial derivatives can be calculated by several methods: an explicit second-order central difference, an explicit sixth-order central difference, an optimized seven-point dispersion-relation-preserving (DRP) method,[23] or the prefactored sixth-order compact scheme and explicit boundary stencils of Hixon.[24] In recent tests, the DRP and prefactored compact schemes proved to be the most accurate for gust-cascade calculations[25]; thus, these two schemes were run and the results compared. A 10th-order explicit filter[26] was used at every stage of the Runge–Kutta solver to provide dissipation. This scheme and code have been extensively validated on benchmark problems, performing very well.

The grid used was a C-H grid topology (Fig. 1), extending at least 10 chord lengths away in each direction. Figure 2 shows the grid near the airfoil surface; the C-grid topology about the airfoil surface can be seen. All grids were generated using the commercial package GridPro.[27] The grid was designed to have a minimum of 10 grid points per wavelength at the highest reduced frequency of inflow disturbance; to minimize the effects of grid variations on the solution, this fine grid was used for all input gusts regardless of the reduced frequency.

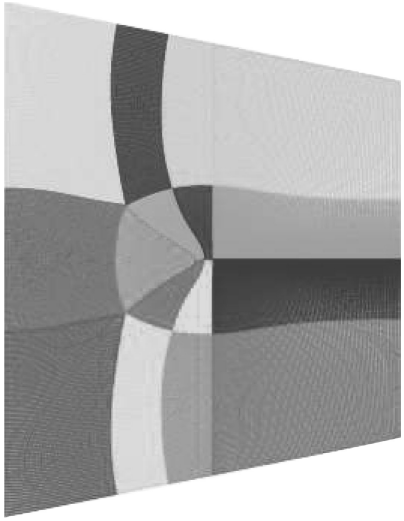

Fig. 1 Grid used for Joukowski airfoil (94,500 points).

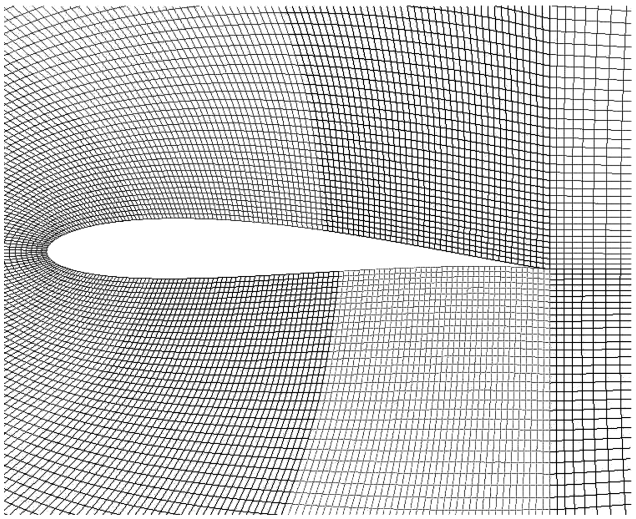

Fig. 2 Close-up of cambered airfoil grid.

BASS is a parallel solver and is designed to automatically distribute the grid topology for efficiency on a parallel cluster.[28] Because so many test cases were run, the code was run in single-processor mode with each case running on a separate processor.

III. Problem Description

In this set of problems, a simple-harmonic vortical gust convects past a 12% thick Joukowski airfoil. The gust has the distribution

$$u_{\text{gust}} = -\left(\epsilon\beta M_\infty \Big/ \sqrt{\alpha^2 + \beta^2}\right)\cos(\alpha x + \beta y - \omega t) \tag{6}$$

$$v_{\text{gust}} = \left(\epsilon\alpha M_\infty \Big/ \sqrt{\alpha^2 + \beta^2}\right)\cos(\alpha x + \beta y - \omega t) \tag{7}$$

For all of the test cases,

$$\epsilon = 0.001, \qquad M_\infty = 0.5 \tag{8}$$

In this work, the inflow disturbance was a two-dimensional gust. The reduced frequency based on the half-chord is defined as

$$k = \omega c/2M_\infty a_\infty \tag{9}$$

where c is the chord length and a is the speed of sound. Using this definition.

$$\alpha = 2k, \qquad \beta = 2k, \qquad \omega = 2kM_\infty \tag{10}$$

Four reduced frequencies were tested: $k = 0.1$, 1.0, 2.0, and 3.0. The nondimensionalized mean flow at infinity is defined as

$$\bar{\rho} = \gamma, \qquad \bar{u} = M_\infty, \qquad \bar{v} = 0, \qquad \bar{p} = 1 \tag{11}$$

Two airfoil geometries are tested in this work. The first geometry is a symmetric airfoil at a zero-deg angle of attack. The second geometry is a cambered airfoil (camber ratio = 0.02) at a two-deg angle of attack.

IV. Initial and Boundary Conditions

For both cases the flow was initialized to the mean flow with the vortical gust superposed at the inflow boundary. At the wall, Hixon's inviscid curvilinear wall boundary condition[29] was used to set the time derivative of the normal momentum to zero at the wall at each Runge–Kutta stage.

At the inflow boundary, the acoustic radiation condition of Tam and Webb[23] was used on the outgoing perturbations. For example, the outgoing u-velocity perturbation u_{BC} was defined as

$$u_{\text{BC}} = u_{\text{boundary}} - \bar{u} - u_{\text{gust}} \tag{12}$$

At the outflow boundaries, Tam and Webb's radiation outflow condition[23] was used with no correction for the outgoing vortical gust.

In these calculations, the flow is assumed to be inviscid (i.e., viscous and heat-transfer effects are neglected). Because the viscous terms in the governing equations are not calculated, this saves computational time and effort. The inviscid flow assumption changes the form of the wall boundary condition from the viscous no-slip condition to the inviscid flow-tangency condition.

It is important to remember that the inviscid wall boundary condition is really setting the inviscid flow tangent to the top of an infinitely thin boundary layer, not to the wall itself. At the point(s) where the boundary layer separates from the wall, the correct boundary condition is for the inviscid flow to remain tangent to the top of the boundary layer, which is not tangent to the wall surface. Thus, the user must somehow set the Kutta condition, which defines the location of the flow separation point on the airfoil.

To set the Kutta condition implicitly, a C-grid topology was used. Figure 2 shows the C-grid topology on the airfoil. At the trailing edge of the airfoil, it can be seen that the grid line which defines the airfoil wall continues into the wake. Because the wall boundary condition uses the wall grid line to define the direction tangent to the wall surface, the flow, which is tangent to the grid line defining the wall, separates from the wall and is shed into the wake.

At the trailing edge, an upper and lower wall condition is calculated, and then the result is averaged; this makes the trailing-edge point single valued. Similarly, the upper and lower wake lines are calculated separately, and the results are averaged. The discontinuity in the boundary condition on the surface line as it enters the wake causes a loss of accuracy near the trailing edge, which is especially apparent for the lifting, high-frequency results. The effect of the trailing-edge discontinuity was much stronger on the cambered lifting airfoil than on the symmetric nonlifting airfoil.

Figures 3 and 4 show a representative result from these test cases. In Fig. 3, the instantaneous disturbance velocity in the y direction is shown for the case of a two-dimensional gust at a reduced frequency of $k = 2.0$ impinging on a cambered airfoil, whereas in Fig. 4 the instantaneous pressure distribution is shown for the same case.

These figures illustrate the performance of the far-field boundary conditions as well as the low dispersion and dissipation errors in the BASS code. In Fig. 3, the gust is introduced at the inflow boundary and is convecting through the other three outflow boundaries. In Fig. 4, the acoustic waves generated by the gust-airfoil interaction are propagating through the boundaries with little reflection.

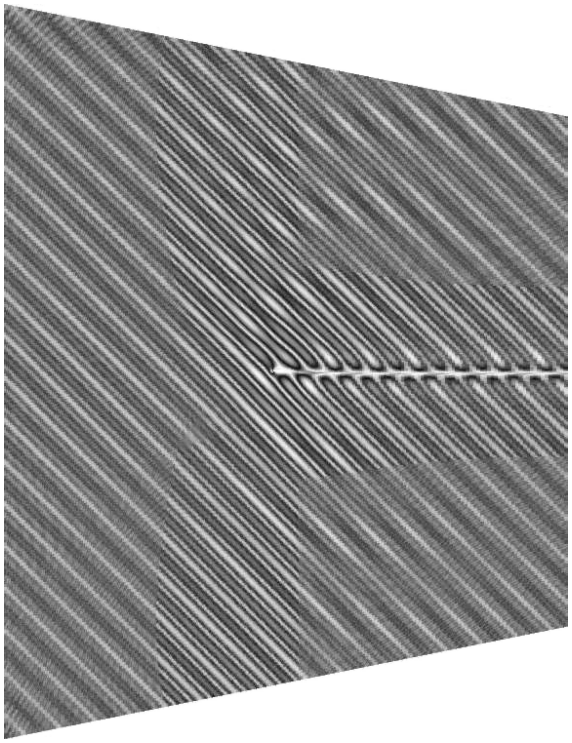

Fig. 3 Instantaneous V velocity distribution ($k = 2.0$, two-dimensional gust, cambered airfoil).

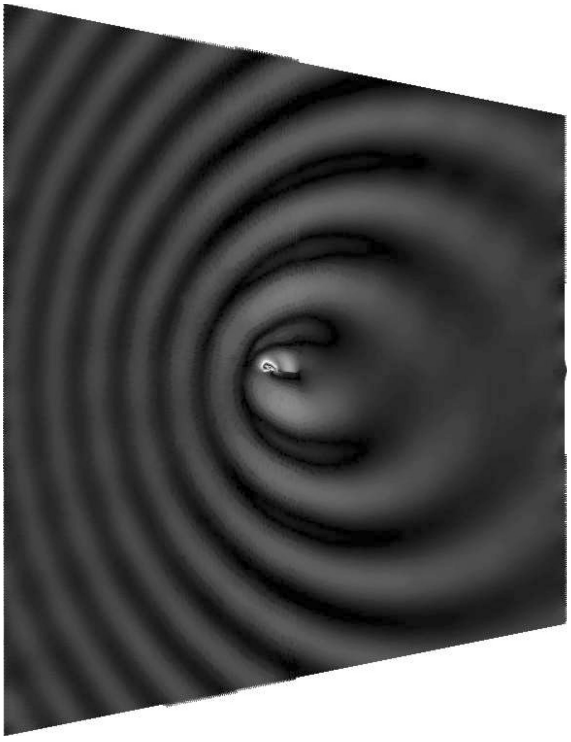

Fig. 4 Instantaneous pressure distribution ($k = 2.0$, two-dimensional gust, cambered airfoil).

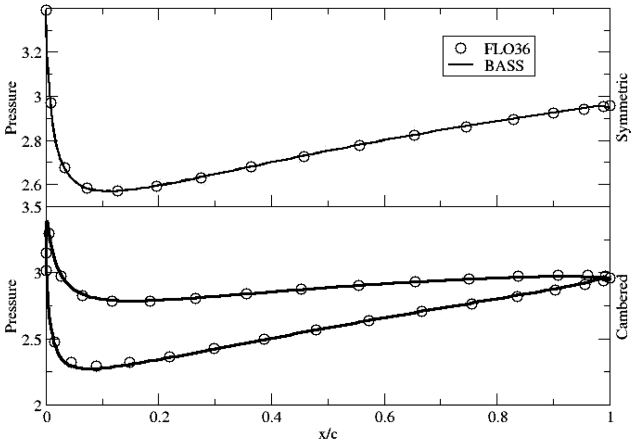

Fig. 5 Mean pressure distribution on the airfoil surface.

V. Results

The BASS code was run to a nondimensional time of 377, requiring 84 h on a 2.8-GHz Intel Pentium IV. In all cases, the prefactored compact sixth-order spatial differencing scheme was used, and 16 solutions per cycle of inflow disturbance were saved. As expected, the nonlifting airfoil case converged faster; however, all cases were run to the same time level. The relatively long computation was performed to ensure that the cases are completely converged for comparison to the benchmark results.

The mean pressures on the airfoil for the two-dimensional gust cases are shown in Fig. 5. The effect of the trailing-edge condition is apparent in both figures; however, the effect is localized near the trailing edge. It is seen that the lifting airfoil peak pressures are slightly overpredicted compared to the FLO36 results; however, the difference is small.

Figures 6 and 7 show the rms pressure disturbance distribution on the airfoil. In Fig. 6, the low-wave-number cases ($k = 0.1$, 1.0)

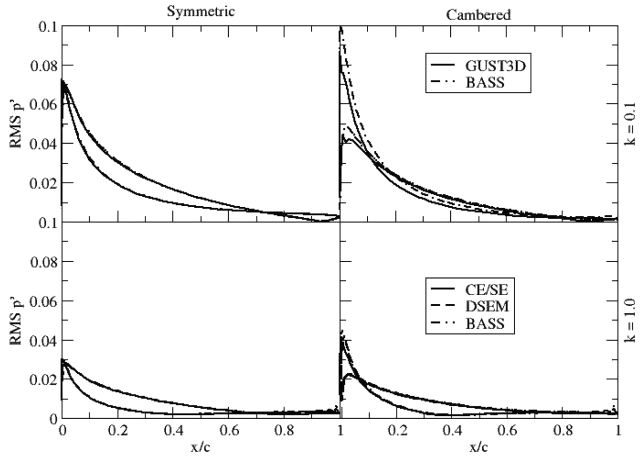

Fig. 6 RMS pressure disturbance distribution on the airfoil surface ($k = 0.1, 1.0$).

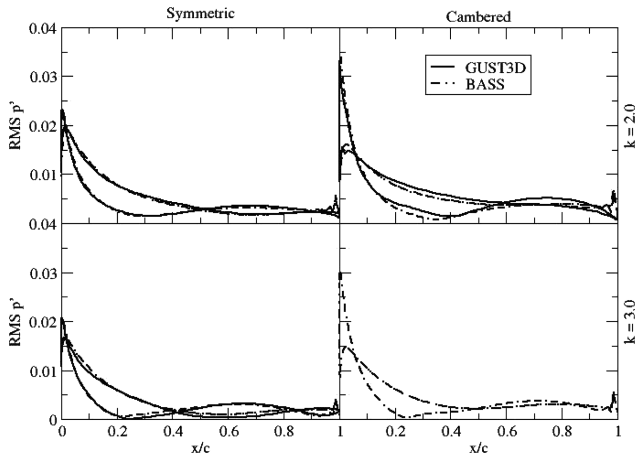

Fig. 7 RMS pressure disturbance distribution on the airfoil surface ($k = 2.0, 3.0$).

are compared to GUST3D results, except in the case of the cambered airfoil, $k = 1.0$ gust. For this case, GUST3D data were not available, and the results are compared to the benchmark solutions of Kopriva's discontinuous spectral element method[30] and to Wang's conservation element/space–time element scheme.[31] The agreement of the BASS solutions with the benchmark results is very good.

In Fig. 7, the high-wave-number cases are shown ($k = 2.0, 3.0$). In the case of the cambered airfoil with a wave number of $k = 3.0$, no results were available to compare to. In all cases, the BASS agreement with the GUST3D results is good.

The trailing-edge condition has some effect on the solution on the airfoil, particularly for the high-frequency gusts. However, as shown in Figs. 6 and 7, the code is predicting the changing pressure distributions for all eight test cases very well, accurately capturing the effects of airfoil geometry and gust-reduced frequency.

Figures 8 and 9 show the acoustic intensity at a distance of one chord length away from the centerpoint of the airfoil. Here the comparison is very good between BASS and GUST3D for the nonlifting low-frequency case and still good for the nonlifting $k = 1.0$ case. Notice that the solution comparison between BASS and GUST3D is better for the nonlifting cases than for the low-frequency loaded airfoil case; research is continuing to resolve the differences in the two solutions. In Fig. 8, data from Golubev's space–time mapping analysis (STMA) benchmark results[32] were used for the lifting airfoil, $k = 1.0$ test case because GUST3D data were not available; for this case, BASS agrees well with the STMA result. In Fig. 9, no data were available for comparison except for one case; in this case, the agreement is adequate.

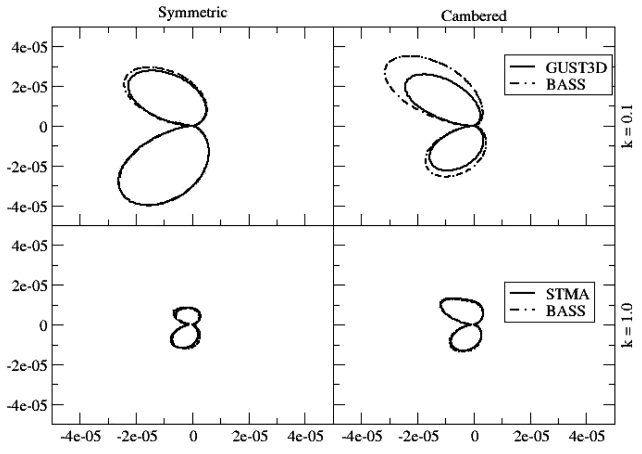

Fig. 8 Acoustic intensity distribution at $R = 1.0$ ($k = 0.1, 1.0$).

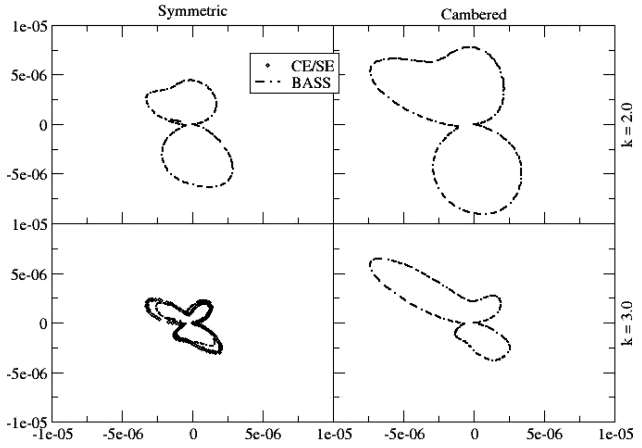

Fig. 9 Acoustic intensity distribution at $R = 1.0$ ($k = 2.0, 3.0$).

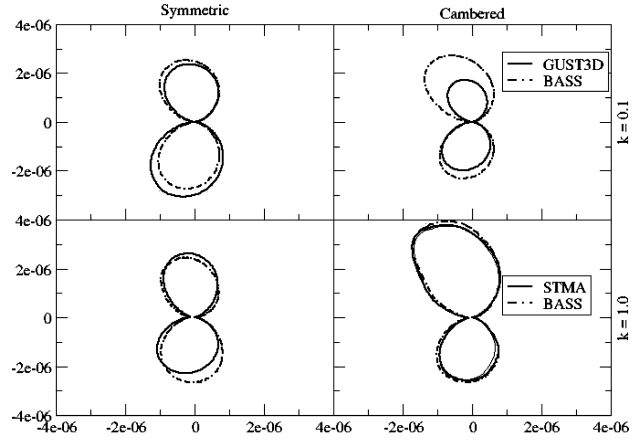

Fig. 10 Acoustic intensity distribution at $R = 4.0$ ($k = 0.1, 1.0$).

Figures 10 and 11 show the acoustic intensity at a distance of four chord lengths away from the centerpoint of the airfoil. The GUST3D solution at this location was obtained using a Kirchhoff approach.[33] Again, the comparisons between BASS and GUST3D are acceptable for the low-frequency nonlifting cases. The discrepancies between the BASS and GUST3D solutions are still evident in the low-frequency lifting airfoil solution, but BASS and STMA compare well for the $k = 1.0$ lifting airfoil solution. In the high-wave-number $k = 3.0$ case, there are boundary reflections that are reducing the accuracy of the computed results. Thus, the $k = 3.0$ data in Fig. 11 are of questionable accuracy and are shown only for completeness.

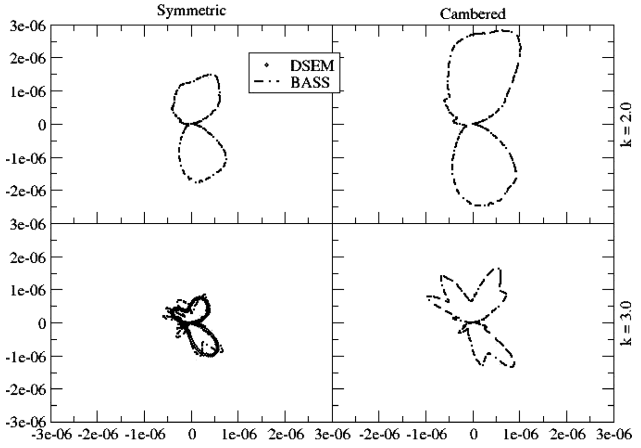

Fig. 11 Acoustic intensity distribution at $R = 4.0$ ($k = 2.0, 3.0$).

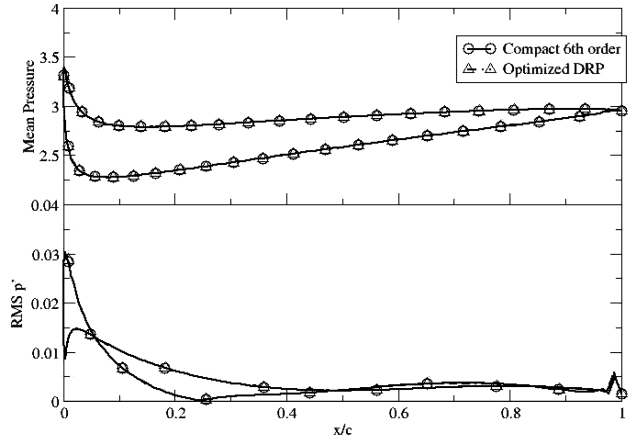

Fig. 12 Effect of spatial differencing scheme on the mean and rms airfoil pressure distribution ($k = 3.0$, cambered airfoil).

VI. Numerical Accuracy

To assess the accuracy of the solution for these cases, three tests were run. In the first test, the results for unsteady pressure throughout the domain were analyzed using a fast Fourier transform. With such low levels of inflow gust excitation, the test case is effectively linear, and the flow unsteadiness should occur only at the inflow gust reduced frequency. In all cases, the amplitude of the flow unsteadiness at the inflow gust reduced frequency was between two and three orders of magnitude higher than any harmonic frequency.

Secondly, the amplitude of the unsteady pressure signal at the inflow gust-reduced frequency was plotted on a logarithmic scale to highlight any spurious sources of noise in the computational domain. This investigation highlighted boundary condition inaccuracies at the highest reduced frequency. In these cases, there were spurious noise sources at the inflow boundary corners as well as at the wake outflow boundary. The spurious noise sources are partially caused by the corner conditions used in BASS and partially caused by the boundary condition itself. However, the lower reduced frequencies did not exhibit this problem.

Finally, the code was run again for all test cases, using the optimized seven-point DRP scheme for spatial differencing rather than the prefactored compact sixth-order scheme. Figures 12 and 13 compare the results for the two schemes at the highest reduced frequency on the cambered airfoil, which is the most numerically demanding test case. Figure 12 shows the mean flow and rms pressure disturbance results on the airfoil surface. Figure 13 shows the acoustic intensity from one to four chord lengths away from the airfoil.

In all cases, the results match very well. Because the two spatial differencing schemes have very different performance at marginal resolution, this leads to the conclusion that the grid density was adequate for these calculations.

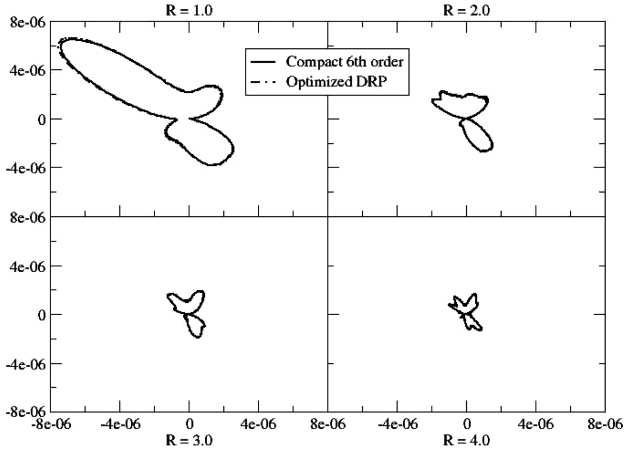

Fig. 13 Effect of spatial differencing scheme on near-field acoustic intensity ($k = 3.0$, cambered airfoil).

VII. Conclusions

A test matrix of eight gust-airfoil interaction problems was solved using a parallelized prefactored sixth-order compact scheme with 10th-order filtering, run on distributed computer clusters. These problems tested the accuracy of the code on stretched, curvilinear grids with nonlinear flows. In all cases, the code was robust and converged well. In these tests, the code predicted the trends and magnitudes of the gust response on the airfoil surface very well for the eight test cases. The near-field acoustic intensity of the gust response was also compared and showed encouraging results for the low reduced frequency cases, while showing some effect from boundary condition reflections at high reduced frequencies. An accuracy study was also performed, and it was found that the solution was effectively grid independent for these calculations.

Acknowledgments

This work was carried out under Grant NAG3-2859 from the NASA Glenn Research Center. Edmane Envia was the Technical Monitor.

References

[1]Tam, C. K. W., "Computational Aeroacoustics: Issues and Methods," *AIAA Journal*, Vol. 33, No. 10, 1995, pp. 1788–1796.

[2]Lele, S. K., "Computational Aeroacoustics: A Review," AIAA Paper 97-0018, Jan. 1997.

[3]Habashi, W. G., Tam, C. K. W., and Morris, P. J., (eds.), "Special Issue: Computational Aeroacoustics," *International Journal of Computational Fluid Dynamics*, Vol. 18, No. 6, 2004, pp. 437–567.

[4]Von Karman, T., and Sears, W. R., "Airfoil Theory for Nonuniform Motion," *Journal of the Aeronautical Sciences*, Vol. 5, No. 10, 1938, pp. 379, 380.

[5]Sears, W. R., "Some Aspects of Non-Stationary Airfoil Theory and Its Practical Applications," *Journal of the Aeronautical Sciences*, Vol. 8, No. 3, 1941, pp. 104–108.

[6]Goldstein, M. E., and Atassi, H. M., "A Complete Second-Order Theory for the Unsteady Flow About an Airfoil Due to a Periodic Gust," *Journal of Fluid Mechanics*, Vol. 74, 1976, pp. 741–765.

[7]Atassi, H. M., "The Sears Problem for a Lifting Airfoil Revisited—New Results," *Journal of Fluid Mechanics*, Vol. 141, 1984, pp. 109–122.

[8]Atassi, H. M., "Unsteady Aerodynamics of Vortical Flows: Early and Recent Developments," *Aerodynamics and Aeroacoustics*, edited by K. Y. Fung, World Scientific, Singapore, 1994, pp. 121–172.

[9]Scott, J. R., and Atassi, H. M., "Numerical Solutions of the Linearized Euler Equations for Unsteady Vortical Flows Around Lifting Airfoils," AIAA Paper 90-0694, Jan. 1990.

[10]Scott, J. R., and Atassi, H. M., "A Finite-Difference, Frequency-Domain Numerical Scheme for the Solution of the Gust-Response Problem," *Journal of Computational Physics*, Vol. 119, June 1995, pp. 75–93.

[11]Hariharan, S. I., Ping, Y., and Scott, J. R., "Time Domain Numerical Calculations of Unsteady Vortical Flows About a Flat Plate Airfoil," *Journal of Computational Physics*, Vol. 101, No. 2, 1992, pp. 419–430.

[12]Lockard, D. P., and Morris, P. J., "A Parallel Implementation of a Computational Aeroacoustic Algorithm for Airfoil Noise," *Journal of Computational Acoustics*, Vol. 5, No. 4, 1997, pp. 337–353.

[13]Lockard, D. P., and Morris, P. J., "The Radiated Noise from Airfoils in Realistic Mean Flows," *AIAA Journal*, Vol. 36, No. 6, 1998, pp. 907–914.

[14]Scott, J. R., "Single Airfoil Gust Response Problem," *Third Computational Aeroacoustics (CAA) Workshop on Benchmark Problems*, NASA CP-2000-209790, 2000, pp. 47–60.

[15]Scott, J. R., "Single Airfoil Gust Response Problem," *Proceedings of the 4th CAA Workshop on Benchmark Problems*, NASA CP-2004-212954, 2003, pp. 45–58.

[16]Jameson, A., and Caughey, D. A., "A Finite Volume Method for Transonic Potential Flow Calculations," AIAA Paper 77-635, June 1977.

[17]Hixon, R., and Mankbadi, R. R., "Validation of a High-Order Prefactored Compact Scheme on Nonlinear Flows with Complex Geometry," *Third Computational Aeroacoustics (CAA) Workshop on Benchmark Problems*, NASA CP-2000-209790, 2000, pp. 117–132.

[18]Sawyer, S., Nallasamy, M., Hixon, R., and Dyson, R. W., "A Computational Aeroacoustic Prediction of Discrete-Frequency Rotor-Stator Interaction Noise—A Linear Theory Analysis," *International Journal of Aeroacoustics*, Vol. 3, No. 1, 2004, pp. 67–86.

[19]Nallasamy, M., Hixon, R., and Sawyer, S., "Computed Linear/Nonlinear Acoustic Response of a Cascade for Single/Multi Frequency Excitation," AIAA Paper 2004-2998, May 2004.

[20]Hixon, R., Shih, S.-H., Dong, T., and Mankbadi, R. R., "Evaluation of Generalized Curvilinear Coordinate Transformations Applied to High-Accuracy Finite-Difference Schemes," AIAA Paper 98-0370, Jan. 1998.

[21]Hu., F. Q., Hussaini, M. Y., and Manthey, J. L., "Low-Dissipation and Low-Dispersion Runge–Kutta Schemes for Computational Acoustics," *Journal of Computational Physics*, Vol. 124, No. 1, 1996, pp. 177–191.

[22]Stanescu, D., and Habashi, W. G., "2N-Storage Low Dissipation and Dispersion Runge–Kutta Schemes for Computational Acoustics," *Journal of Computational Physics*, Vol. 143, No. 2, 1998, pp. 674–681.

[23]Tam, C. K. W., and Webb, J. C., "Dispersion-Relation-Preserving Finite Difference Schemes for Computational Acoustics," *Journal of Computational Physics*, Vol. 107, No. 2, 1993, pp. 262–281.

[24]Hixon, R., "Prefactored Small-Stencil Compact Schemes," *Journal of Computational Physics*, Vol. 165, No. 2, 2000, pp. 522–541.

[25]Hixon, R., Nallasamy, M., Sawyer, S., and Dyson, R., "Comparison of Numerical Schemes for a Realistic Computational Aeroacoustics Benchmark Problem," *International Journal of Aeroacoustics*, Vol. 3, No. 4, 2004, pp. 379–398.

[26]Kennedy, C. A., and Carpenter, M. H., "Several New Numerical Methods for Compressible Shear-Layer Simulations," *Applied Numerical Mathematics*, Vol. 14, No. 4, 1994, pp. 397–433.

[27]GridPro™/az3000, Program Development Corp., White Plains, NY, 1996.

[28]Sharif, R., and Hixon, R., "A Sub-Optimal Load Balancing Strategy for a Heterogeneous Cluster of PCs," AIAA Paper 2004-1089, Jan. 2004.

[29]Hixon, R., "Curvilinear Wall Boundary Conditions for Computational Aeroacoustics," AIAA Paper 99-2395, June 1999.

[30]Rasetarinera, P., Kopriva, D. A., and Hussaini, M. Y., "Discontinuous Spectral Element Solution of Aeroacoustic Problems," *Third Computational Aeroacoustics (CAA) Workshop on Benchmark Problems*, NASA CP-2000-209790, 2000, pp. 103–115.

[31]Wang, X.-Y., Himansu, A., Chang, S.-C., and Jorgenson, P. C. E., "Applications of the Space-Time Conservation Element and Solution Element (CE/SE) Method to Computational Aeroacoustic Benchmark Problems," *Third Computational Aeroacoustics (CAA) Workshop on Benchmark Problems*, NASA CP-2000-209790, 2000, pp. 133–159.

[32]Golubev, V. V., Mankbadi, R. R., and Scott, J. R., "Numerical Inviscid Analysis of Nonlinear Airfoil Response to Impinging High-Intensity High-Frequency Gust," AIAA Paper 2004-3002, May 2004.

[33]Hariharan, S. I., Scott, J. R., and Krieder, K. L., "A Potential-Theoretic Method for Far-Field Sound Radiation Calculations," *Journal of Computational Physics*, Vol. 164, No. 1, 2000, pp. 143–161.

H. Atassi
Associate Editor